Optik - International Journal for Light and Electron Optics 247 (2021) 167998

Contents lists available at ScienceDirect

Optik

journal homepage: www.elsevier.com/locate/ijleo

Original research article

Modeling and correction of pointing error of space-borne optical imager

B. Huang [a,b,*], Z.H. Li [a], X.Z. Tian [a], L. Yang [a], P.J. Zhang [a], B. Chen [a]

[a] Changchun Institute of Optics, Fine Mechanics and Physics, Chinese Academy of Science, Changchun 130031, Jilin, China
[b] University of Chinese Academy of Science, Beijing 100039, China

ARTICLE INFO

Keywords:
Space-borne optical imager
Pointing error
Monte-Carlo method
Transformation matrix calibration
Error correction

ABSTRACT

Pointing error is one of the most critical performance indices of space-borne optical imager and is of great significance for optical imaging and target tracking. In order to correct the pointing error of an optical imager and make it meet the design requirement, first of all, the mathematical model of the relation of pointing error and assembly errors of mechanical components is established, acquiring the analytical expressions of pitch angle and azimuth angle of the 2-DOFs pointing mechanism. Then, the mathematical model of transformation matrix calibration of coordinate systems is set up and the calculation formulas of transformation matrix and angular deviation are provided. Moreover, the simulation model of pointing error is built based on Monte-Carlo method given that the distribution of each assembly error satisfies normal assumption, together with the distribution of pointing error before and after assembly error correction. Finally, the correction test of pointing error is accomplished and test results before and after correction are compared, demonstrating that the maximum of compensated value is 26″ and the minimum is 6″ and the pointing accuracy has increased by 64% in average. After correction, the total pointing error of imager is no more than 20″ which meets the system performance requirement.

1. Introduction

Space-borne optical remote sensors have developed rather rapidly in aerospace industry across the world due to the availability in large-scale and long-time observation of space environment, solar corona, space weather and some other space areas. The observation data is playing a notably important role in astronomy and geology. As is known, the main optical axis of an optical imager is inevitably deviated from its theoretical position and attitude due to the errors induced by manufacturing and assembly, which is called pointing error. Pointing error, one of the most crucial performance indices, has an extremely influence on the performance of an optical system.

Pointing error is mainly resulted from assembly errors induced in the assembly process of mechanical rotating axes. The assembly errors can lead to angular deviation and transformation matrix between two local coordinate systems of rotating axes, thus resulting in the pointing error. In order to eliminate the negative influence of assembly errors on the pointing error of a system, a precise and strict assembling process is needed. After assembling, the real assembly errors need to be calibrated so as to be compensated in the control system and finally pointing error can be corrected to be within the range of performance requirement.

Considerable progress has been made in the fields of error model and error calibration by institutes and scholars all over the world.

* Corresponding author at: Changchun Institute of Optics, Fine Mechanics and Physics, Chinese Academy of Science, Changchun 130031, Jilin, China.
E-mail address: huangbin@ciomp.ac.cn (B. Huang).

https://doi.org/10.1016/j.ijleo.2021.167998
Received 2 July 2021; Received in revised form 30 August 2021; Accepted 15 September 2021
Available online 20 September 2021

In the research and developing process of some optical remote sensors, one or two theodolites, namely a simplified method, are used to calibrate the relative attitude and angular deviation of components [1–4]. However, this method cannot get directly the transformation matrix of two coordinate systems, neither can absolute angular deviation be provided, which has an extremely negative influence on the compensated accuracy and final performance. Wu and Su adopt a measurement method based on visualization of theodolites [5], while Zhang has developed a calibration system with high accuracy of theodolites and large field of view of camera by integrating a theodolite and a camera [6]. Moreover, Forbes and et al. accomplished a comparison of calibration methods available in the area of error calibration, which illustrates that theodolites are much more effective in calibration than laser distance measuring device [7]. What is more, calibration methods with the use of theodolites are also taken advantage of in 3D imaging due to the need of coordinate calculations and coordinate transformation [8–10]. However, the majority of the work mentioned above can only offer a less precise calibration result because of enough number of theodolites not being employed. When the absolute angular deviation and transformation matrix are desired, four theodolites at least are necessary to build up an absolute optical reference so that a much more precise angular deviation and coordinate transformation matrix can be acquired, which is the main part of this paper.

Pointing error is a key problem in the field of optics, including the field of space-borne optical remote sensing, free optics communication and so forth [11–13]. Ding and et al. established some experimental platforms to analyze the pointing error of the free optics communication instrument and validated the correctness of the compensation method [14]. Tan and et al. did some research on the relation between temperature distribution and pointing error for inter-satellite [15]. Some more work was conducted concerning the effect of pointing error on communication efficiency and system performance [16–20]. In addition to the ground-based optical communication, some research on underwater free optics communication was conducted to figure out the influence of depth in the water on the efficiency of communication and the pointing accuracy [21]. Some other correction methods were developed in recent years across researchers all over the world to solve the pointing error in space-borne optics and ground-based laser communication. A correction method of pointing error for a theodolite is presented in [22], in which movement errors of rotating axes and positioning errors of encoders are taken into account. An analysis of pointing error of Risley-prism-based beam system is performed in [23], also evaluating the allowance of errors for a given pointing accuracy. Correction methods for pointing errors caused by geometric and nonlinear errors are focused in [24,25]. However, little attention was paid in the work mentioned above on the mathematical model of relation between pointing error and assembly errors in the optical system, which is another important part in this paper.

In order to identify the pointing error of a space-borne optical imager and correct the error, a mathematical model of pointing error is firstly proposed in this paper to illustrate that it is the assembly errors but not the geometric errors that have a considerable influence on the pointing error and demonstrate the relation between pointing errors and assembly errors, which is the first part of novel and important work. Secondly, a calibration method of transformation matrix of coordinate systems is presented to help build up an absolutely optical reference and acquire the angular deviation of two coordinate systems, which improves the calibration accuracy quite much. This part of work is another novel and important one. Thirdly, after getting the mathematical model, a simulation model based on Monte-Carlo Method is built up to obtain the probable range of pointing error when all the assembly errors are regarded as the probabilistically normal distribution, primarily verifying the effectiveness of the abovementioned mathematical models. At last, a correction test of pointing error is conducted, validating the correctness and effectiveness of all the mathematical models and calibration methods proposed in this paper. All of the abovementioned work contributes together to modeling, analyzing and correcting the pointing error of the space-borne optical imager put forward in this manuscript.

The remainder of this paper is organized as follows. In Section 2, the space-borne optical imager and its technical indices are introduced, including its components and coordinate systems which are employed to describe the relative positions and attitude of all the components. A mathematical model of pointing error is put forward in Section 3, figuring out the quantitative relation between the pointing error and all the assembly errors and laying a foundation for the subsequent simulation work as well. Also the mathematical model of transformation matrix calibration of coordinate systems is put forward in this section. In Section 4, a simulation model of pointing error is built up and a correction test of pointing error is conducted in Section 5. Consequently, a conclusion is drawn in Section 6.

2. Optical-mechanical system

2.1. System requirement

A space-borne optical imager is employed to capture the solar X-ray and extreme ultra-violet (EUV) spectrum, predicting the influence of solar corona on the space weather and earth weather. Therefore, the major functions are as follows. The pointing accuracy of the imager must be better than 20″to realize all the functions.

a) Pointing and aligning with two degrees of freedom (DOF);
b) Capturing and imaging the solar X-ray and EUV spectrum;
c) Scanning and searching sun in a large field of view;
d) Tracking sun in a small field of view.

2.2. System composition

The optical imager comprises a pointing mechanism with two DOFs, a camera that images solar X-ray and EUV spectrum and guiding telescopes. The pointing mechanism consists of a pitching rotating axis and an azimuth rotating axis. The major components

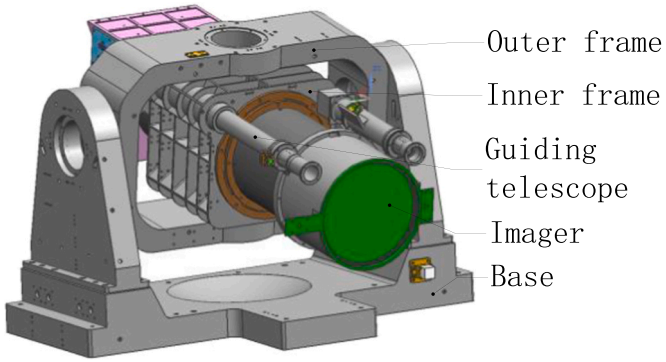

Fig. 1. Optical-mechanical model.

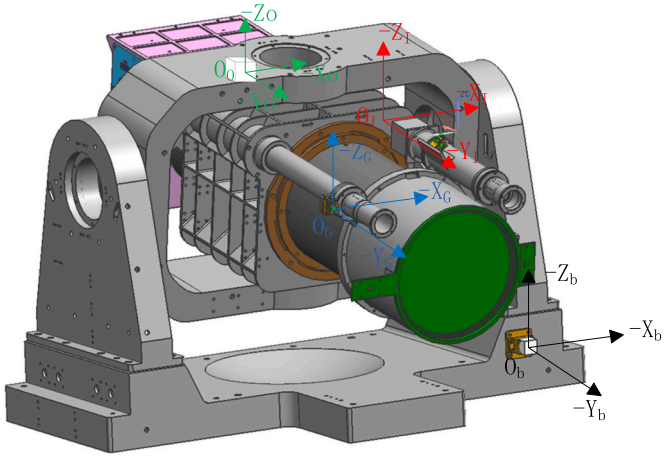

Fig. 2. Illustration of coordinate systems.

are specified in Fig. 1.

The working principle of the optical imager is briefly presented. According to the engineering requirements, the imager is mounted on the outer deck of the satellite. When the imager starts to work in the space, the outer frame can rotate along the pitching axis and the inner frame can rotate along the azimuth axis hence the camera and the guiding telescopes are able to rotate in two DOFs since they are mounted on the inner frame, thus realizing the sun search and tracking.

2.3. System coordinate systems

In order to describe the relative position and attitude between the target and different components, precise cubic prisms are placed respectively on the base, outer frame, inner frame and guiding telescope to be the optical reference so that local coordinate systems are built up on the prisms, which is the prerequisite for the calibration of assembly error and correction of pointing error. Positions of all the prisms are shown in Fig. 2.

where.

O_B-$X_BY_BZ_B$: the coordinate system of base;

O_O-$X_OY_OZ_O$: the coordinate system of outer frame;

O_I-$X_IY_IZ_I$: the coordinate system of inner frame;

O_G-$X_GY_GZ_G$: the coordinate system of guiding telescope.

In the sun searching stage, the coordinate of sun in the coordinate system of satellite platform is provided by the satellite broadcast. The transformation matrix between coordinate system of base of the optical imager and that of satellite can be calibrated, then the pitch and azimuth angles used to capture the sun can be calculated after a series of coordinate transformation and inverse kinematics.

3. Modeling and formulation

3.1. Mathematical model of pointing error

According to the theory of coordinate transformation matrix, in the sun-searching stage, the coordinates of sun in coordinate system of satellite and in coordinate system of guiding telescope satisfy Eq. (1).

$$\begin{pmatrix} X_{\text{sun}} \\ Y_{\text{sun}} \\ Z_{\text{sun}} \end{pmatrix} = \mathbf{T}_{\text{B}}^{\text{SP}} \cdot \mathbf{T}_{\text{O}}^{\text{B}} \cdot \mathbf{T}_{\text{I}}^{\text{O}} \cdot \mathbf{T}_{\text{G}}^{\text{I}} \cdot \mathbf{P}_{\text{S}}^{\text{G}} \tag{1}$$

$(X_{\text{sun}} \quad Y_{\text{sun}} \quad Z_{\text{sun}})^{\text{T}}$ represents the vector coordinate of sun in satellite platform coordinate system, which can be acquired from satellite broadcast.

$\mathbf{T}_{\text{B}}^{\text{SP}}$ is the transformation matrix from coordinate system of satellite platform to that of the base. Due to assembly errors, there exist angular deviations between coordinate systems of satellite platform and base, which is denoted by $(\alpha_1,\beta_1,\gamma_1)$. So $\mathbf{T}_{\text{B}}^{\text{SP}}$ is specified in Eq. (2).

$$\mathbf{T}_{\text{B}}^{\text{SP}} = \begin{bmatrix} \cos\gamma_1 & -\sin\gamma_1 & 0 \\ \sin\gamma_1 & \cos\gamma_1 & 0 \\ 0 & 0 & 1 \end{bmatrix} \begin{bmatrix} 1 & 0 & 0 \\ 0 & \cos\alpha_1 & -\sin\alpha_1 \\ 0 & \sin\alpha_1 & \cos\alpha_1 \end{bmatrix} \begin{bmatrix} \cos\beta_1 & 0 & \sin\beta_1 \\ 0 & 1 & 0 \\ -\sin\beta_1 & 0 & \cos\beta_1 \end{bmatrix} \tag{2}$$

According to the requirements of assembling and aligning, every one of the assembly errors above is no more than 6′, so Eq. (2) can be simplified as Eq. (3) since $\sin\theta \approx \theta$ and $\cos\theta \approx 1$.

$$\mathbf{T}_{\text{B}}^{\text{SP}} = \begin{bmatrix} 1 & -\gamma_1 & \beta_1 \\ \gamma_1 & 1 & -\alpha_1 \\ -\beta_1 & \alpha_1 & 1 \end{bmatrix} \tag{3}$$

$\mathbf{T}_{\text{O}}^{\text{B}}$ denotes the transformation matrix from coordinate system of base to that of outer frame. There exist a relative rotation and an assembly deviation between outer frame and base, and the transformation matrix of relative rotation is

$${}^{1}\mathbf{T}_{\text{O}}^{\text{B}} = \begin{bmatrix} 1 & 0 & 0 \\ 0 & \cos E & -\sin E \\ 0 & \sin E & \cos E \end{bmatrix} \tag{4}$$

Where $E = \omega_{\text{E}} \cdot t$ is the working angle of pitch axis, ω_{E} is the angular velocity of pitch axis.

The assembly error of outer frame relative to base is similar to Eq. (2), so the deviation matrix is as follows assuming that the angular deviation is $(\alpha_2,\beta_2,\gamma_2)$

$${}^{2}\mathbf{T}_{\text{O}}^{\text{B}} = \begin{bmatrix} 1 & -\gamma_2 & \beta_2 \\ \gamma_2 & 1 & -\alpha_2 \\ -\beta_2 & \alpha_2 & 1 \end{bmatrix} \tag{5}$$

Therefore, the total transformation matrix between outer frame and base is

$$\mathbf{T}_{\text{O}}^{\text{B}} = {}^{2}\mathbf{T}_{\text{O}}^{\text{B}} \cdot {}^{1}\mathbf{T}_{\text{O}}^{\text{B}} \tag{6}$$

$\mathbf{T}_{\text{I}}^{\text{O}}$ denotes the transformation matrix from coordinate system of outer frame to that of inner frame. It is assumed that pitch axis is absolutely perpendicular to azimuth axis and there is only a relative rotation between inner frame and azimuth axis, so the transformation matrix is

$$\mathbf{T}_{\text{I}}^{\text{O}} = \begin{bmatrix} \cos A & -\sin A & 0 \\ \sin A & \cos A & 0 \\ 0 & 0 & 1 \end{bmatrix} \tag{7}$$

Where $A = \omega_{\text{A}} \cdot t$ is the working angle of azimuth axis, ω_{A} is the angular velocity of azimuth axis.

$\mathbf{T}_{\text{G}}^{\text{I}}$ denotes the transformation matrix from coordinate system of inner frame to that of guiding telescope. Assuming that the assembly error of guiding telescope relative to inner frame is $(\alpha_3,\beta_3,\gamma_3)$, then

$$\mathbf{T}_{\text{G}}^{\text{I}} = \begin{bmatrix} 1 & -\gamma_3 & \beta_3 \\ \gamma_3 & 1 & -\alpha_3 \\ -\beta_3 & \alpha_3 & 1 \end{bmatrix} \tag{8}$$

$\mathbf{P}_{\text{S}}^{G}$ denotes the vector coordinate of sun in coordinate system of guiding telescope. When the sun lies in the center of field of view of guiding telescope, $\mathbf{P}_{\text{S}}^{G} = (0 \ -1 \ 0)$.

After combining equations from (1) to (8), the analytical expression of pitch angle and azimuth angle can be acquired. First of all, assume that

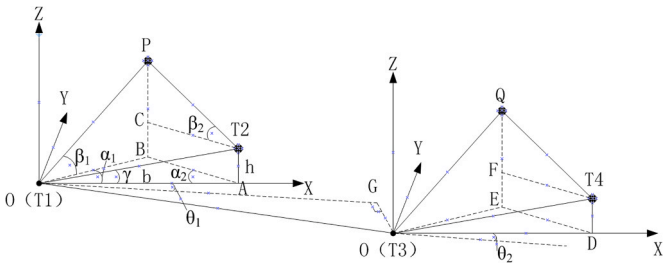

Fig. 3. Scheme of relative position.

$$\begin{pmatrix} b_1 \\ b_2 \\ b_3 \end{pmatrix} = \begin{bmatrix} 1 & -(\gamma_1+\gamma_2) & \beta_1+\beta_2 \\ \gamma_1+\gamma_2 & 1 & -(\alpha_1+\alpha_2) \\ -(\beta_1+\beta_2) & \alpha_1+\alpha_2 & 1 \end{bmatrix}^{-1} \begin{pmatrix} X_{\text{sun}} \\ Y_{\text{sun}} \\ Z_{\text{sun}} \end{pmatrix} \tag{9}$$

$$\begin{pmatrix} a_1 \\ a_2 \\ a_3 \end{pmatrix} = \begin{pmatrix} \gamma_3 \\ -1 \\ -\alpha_3 \end{pmatrix} \tag{10}$$

Then,

$$\begin{cases} A = \arcsin \dfrac{b_1}{\sqrt{a_2^2+a_1^2}} - \arctan \dfrac{a_1}{a_2} \\ E = -\arcsin \dfrac{a_3}{\sqrt{b_2^2+b_3^2}} + \arctan \dfrac{b_3}{b_2} \end{cases} \tag{11}$$

Without considering all the assembly errors analyzed above, Eq. (11) can be simplified as

$$\begin{cases} A = \arcsin X_{\text{sun}} \\ E = \arctan \dfrac{Z_{\text{sun}}}{Y_{\text{sun}}} \end{cases} \tag{12}$$

3.2. Mathematical model of transformation matrix calibration

It is Obvious that $(\alpha_i, \beta_i, \gamma_i)(i = 1, 2, 3)$ are the main sources of pointing error. Therefore, in order to correct the pointing error, transformation matrices between satellite platform and base, base and outer frame, inner frame and guiding telescope need to be calibrated and assembly errors need to be compensated.

Each precise cubic prism mounted on the component is used to be the optical reference, on which a local coordinate system is built up. To calibrate the angular deviation between two components, four theodolites are in need. The relative position between theodolites and prisms is shown in Fig. 3.

Fig. 3 is explained in detail as follows. Without losing generality, it is assumed that four theodolites are placed on positions T1, T2, T3, and T4, among which T1 and T2 are used to calibrate the cubic prism P and the other two for cubic prism Q. The point T1 in the figure stands for the intersection point of the azimuth axis and pitch axis of the theodolite T1 and the same for point T2. Then, the segment T1T2 is projected on the horizontal plane to obtain a new line through point T1, which is the X-axis. Furthermore, a vertical line through point T1 can be easily acquired, which is the Z-axis. Y-axis can be calculated by vector product of X-axis and Z-axis. Now the coordinate system T1-XYZ is realized whose origin is point T1 and three coordinate axes are all specified above. The process is the same for T3-XYZ.

Furthermore, α_1 denotes the azimuth angle of theodolite T1; α_2 is the azimuth angle of T2; β_1 is the pitch angle of T1; β_2 is the pitch angle of T2; γ is the pitch angle of T1 mutual collimation with T2.

Next, the coordinate system of cubic prism is built. Given some geometric relations in coordinate system T1-XYZ, the coordinate of point P can be easily acquired

$$\begin{cases} x_p = OP \cdot \cos\beta_1 \cdot \cos\alpha_1 \\ y_p = OP \cdot \cos\beta_1 \cdot \sin\alpha_1 \\ z_p = OP \cdot \sin\beta_1 \end{cases} \tag{13}$$

The coordinate of vector PT1 and PT2 is also known

$$\begin{cases} \overrightarrow{\mathbf{PT1}} = \left(-x_p, -y_p, -z_p\right) \\ \overrightarrow{\mathbf{PT2}} = \left(b - x_p, -y_p, h - z_p\right) \end{cases} \tag{14}$$

Theoretically, PT1 and PT2 can be used to represent the X-axis and Y-axis of the coordinate system of cubic prism P since they are the normal lines of two adjacent surfaces of a cube. However, due to the error of perpendicularity of a cubic prism, an extra vector product calculation is necessary to avoid the impact caused by this perpendicularity error. In this paper, PT1 is chosen to be the X-axis and PT2 represents the pseudo-Y-axis. In that case, Z-axis can be calculated

$$\mathbf{Z}-\mathbf{axis}=\begin{vmatrix} i & j & k \\ -x_p & -y_p & -z_p \\ b-x_p & -y_p & h-z_p \end{vmatrix}=\begin{pmatrix} -hy_p, hx_p-bz_p, by_p \end{pmatrix} \tag{15}$$

Then the theoretically accurate Y-axis can be obtained

$$\mathbf{Y}-\mathbf{axis}=\begin{vmatrix} i & j & k \\ -hy_p & hx_p-bz_p & by_p \\ -x_p & -y_p & -z_p \end{vmatrix}=\begin{pmatrix} by_p^2+bz_p^2-hx_pz_p, -bx_py_p-hy_pz_p, hy_p^2+hx_p^2-bx_pz_p \end{pmatrix} \tag{16}$$

Given the directional vectors of three coordinate axes, the coordinate system of cubic prism P can be acquired after the normalization of directional vectors.

$$\begin{cases} \mathbf{P}:\mathbf{X}=\dfrac{\left(-x_p,-y_p,-z_p\right)}{\left|\left(-x_p,-y_p,-z_p\right)\right|} \\ \mathbf{P}:\mathbf{Y}=\dfrac{\left(by_p^2+bz_p^2-hx_pz_p,-bx_py_p-hy_pz_p,hy_p^2+hx_p^2-bx_pz_p\right)}{\left|\left(by_p^2+bz_p^2-hx_pz_p,-bx_py_p-hy_pz_p,hy_p^2+hx_p^2-bx_pz_p\right)\right|} \\ \mathbf{P}:\mathbf{Z}=\dfrac{\left(-hy_p,hx_p-bz_p,by_p\right)}{\left|\left(-hy_p,hx_p-bz_p,by_p\right)\right|} \end{cases} \tag{17}$$

where P:X represents the X-axis of cubic prism P; $|\bullet|$ represents the norm of a vector.

It is apparent that all the calculation process is as well suitable for cubic prism Q.

The transformation matrix from coordinate system T1-XYZ to cubic prism P can be easily acquired just by projecting three axes of P coordinate system respectively on T1-XYZ, as is shown in Eq. (18).

$$\mathbf{T}_{\mathrm{P}}^{\mathrm{T1}}=\begin{bmatrix} \mathrm{P:X}\cdot(1\,0\,0) & \mathrm{P:Y}\cdot(1\,0\,0) & \mathrm{P:Z}\cdot(1\,0\,0) \\ \mathrm{P:X}\cdot(0\,1\,0) & \mathrm{P:Y}\cdot(0\,1\,0) & \mathrm{P:Z}\cdot(0\,1\,0) \\ \mathrm{P:X}\cdot(0\,0\,1) & \mathrm{P:Y}\cdot(0\,0\,1) & \mathrm{P:Z}\cdot(0\,0\,1) \end{bmatrix} \tag{18}$$

In Fig. 3, due to the parallel of the Z-axis of theodolite T1 and T3, the transformation matrix of these two theodolites can be obtained by just figuring out the Euler angle on Z-axis. It is assumed that $\theta 1 > \theta 2$, without losing generality, and the Euler angle on Z-axis between theodolite T1 and T3 is

$$\theta=\theta_1-\theta_2 \tag{19}$$

Then the transformation matrix between these two theodolites is

$$\mathbf{T}_{\mathrm{T3}}^{\mathrm{T1}}=Rot\begin{pmatrix} z, -\theta \end{pmatrix}=\begin{bmatrix} \cos\theta & \sin\theta & 0 \\ -\sin\theta & \cos\theta & 0 \\ 0 & 0 & 1 \end{bmatrix} \tag{20}$$

Given all the calculation results presented above, the transformation matrix from cubic prism P to Q can be acquired by transforming the coordinate system from P to T1, then from T1 to T3, and from T3 to Q in the last. Therefore, the transformation matrix from P to Q is

$$\mathbf{T}_{\mathrm{Q}}^{\mathrm{P}}=\mathbf{T}_{\mathrm{T1}}^{\mathrm{P}}\cdot\mathbf{T}_{\mathrm{T3}}^{\mathrm{T1}}\cdot\mathbf{T}_{\mathrm{Q}}^{\mathrm{T3}}=\left(\mathbf{T}_{\mathrm{P}}^{\mathrm{T1}}\right)^{-1}\cdot\mathbf{T}_{\mathrm{T3}}^{\mathrm{T1}}\cdot\mathbf{T}_{\mathrm{Q}}^{\mathrm{T3}} \tag{21}$$

3.3. Angular deviation of transformation matrix

It is known that the transformation matrix is Eq. (2) when there exists an angular deviation on all the three directions and the transformation matrix T can be calculated by Eq. (21), then

$$\mathbf{T}=\begin{bmatrix} a_{11} & a_{12} & a_{13} \\ a_{21} & a_{22} & a_{23} \\ a_{31} & a_{32} & a_{33} \end{bmatrix} \tag{22}$$

Then the angular deviation of two coordinate systems can be acquired given Eqs. (2) and (22).

Table 1
Details of assembly errors.

Error item	Error description	Maximum	Distribution
$(\alpha_1,\beta_1,\gamma_1)$	Satellite platform and base	6′	Normal distribution
$(\alpha_2,\beta_2,\gamma_2)$	Base and outer frame	1′	
$(\alpha_3,\beta_3,\gamma_3)$	Inner frame and guiding telescope	1′	

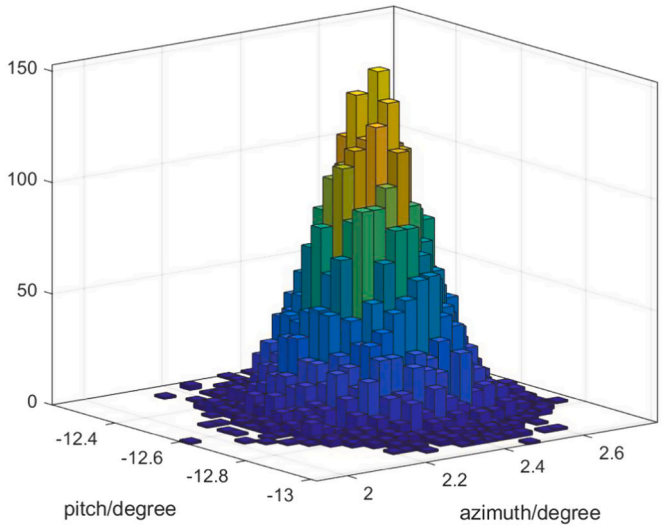

Fig. 4. Simulation result of pitch and azimuth angle.

$$\begin{cases} \alpha = arc\sin(a_{32}) \\ \beta = -\arctan(a_{31}/a_{33}) \\ \gamma = -\arctan(a_{12}/a_{22}) \end{cases} \tag{23}$$

4. Numerical simulation

4.1. Distribution of assembly error

It is known that there exist assembly errors among satellite platform and all the components of the optical imager. A tolerance allocation is fulfilled at the beginning of system design. However, the final pointing error is not an algebraic summation of all the assembly errors, but a probabilistic distribution. Therefore, the probabilistic distribution of every one of the errors above needs to be analyzed, ensuring that the final pointing error is within the range of system requirement. The details of all the errors are shown in Table 1.

4.2. Monte-Carlo method

Monte-Carlo method is based on the statistical characteristic of variables and replaces constant with variable, which leads to the final simulation result much closer to the reality than any other simulation method. Since there are a considerable number of error variables in the system which all satisfy normal distribution, Monte-Carlo method is adopted to accomplish the error analysis.

Without losing generality, the vector coordinate of the sun in coordinate system of satellite platform is assumed to be Eq. (24) which is regarded as the input for the whole simulation process.

$$(X_{\text{sun}} \quad Y_{\text{sun}} \quad Z_{\text{sun}})^{\text{T}} = (0.042 \quad -0.975 \quad 0.218)^{\text{T}} \tag{24}$$

4.3. Simulation result before correction

The simulation model of pointing error is established in MatLab, then the theoretical pitch angle and azimuth angle can be obtained when no assembly error is taking into consideration, namely

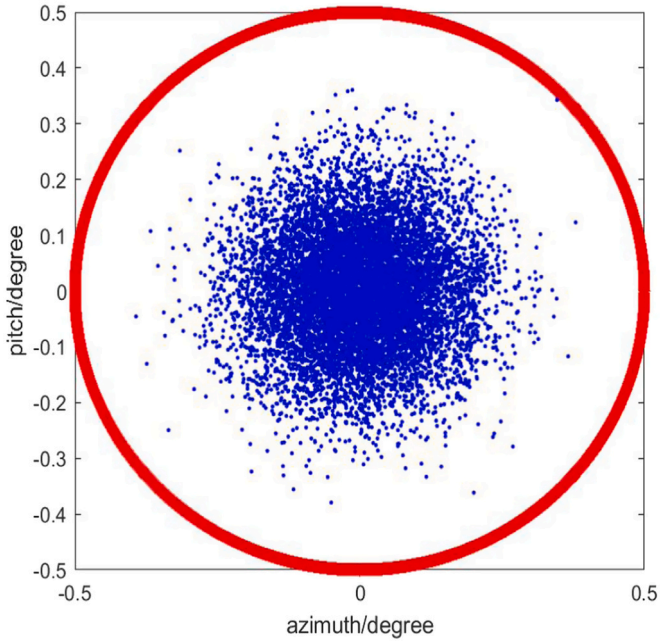

Fig. 5. Distribution of deviation.

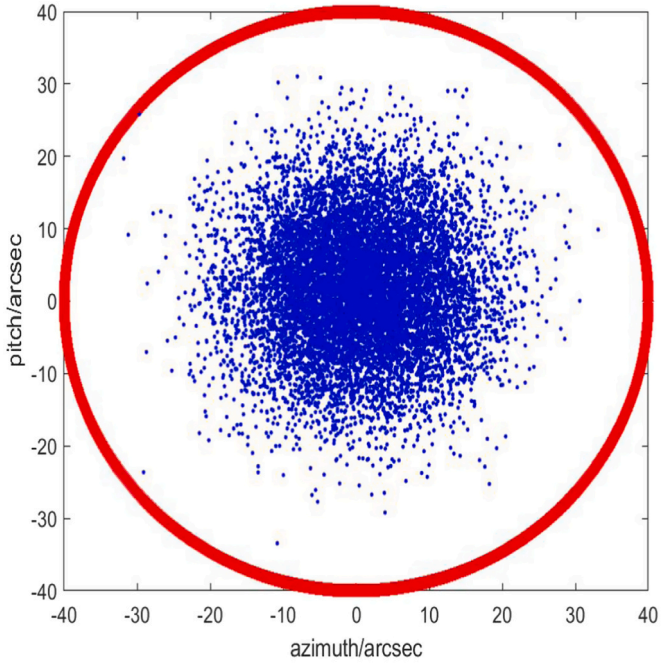

Fig. 6. Distribution of residual error after correction.

$$\begin{cases} A = 2.407^\circ \\ E = -12.604^\circ \end{cases} \tag{25}$$

When all the assembly errors are taken into account, the simulation result of pitch angle and azimuth angle is shown in Fig. 4 which illustrates that the majority of data are close to the theoretical result, in accordance with normal distribution.

The deviation of simulation data from theoretical result is shown in Fig. 5, which demonstrates that pointing error is distributed probabilistically normally within the range of $\pm 0.5^\circ$, far more than the system requirement of pointing accuracy. Hence, it is indispensable to calibrate all the assembly errors and correct them in the control system.

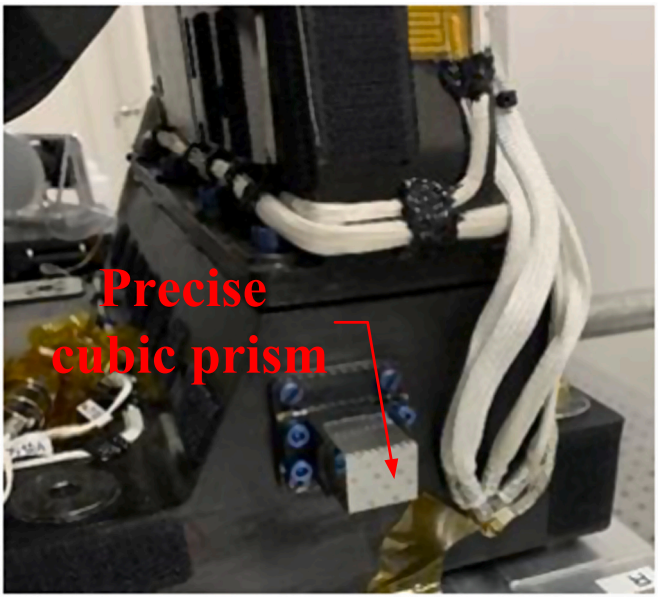

Fig. 7. Mounting status of cubic prism.

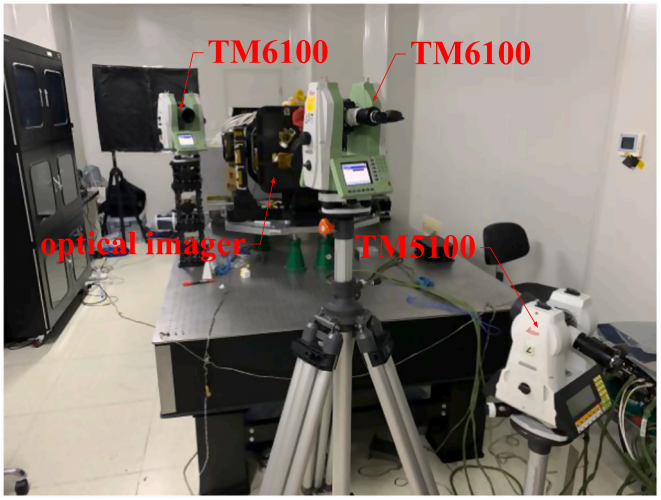

Fig. 8. Working position of theodolites.

4.4. Simulation result after correction

According to the simulation results, each assembly error does have a noticeably negative impact on the pointing accuracy. After calibration and correction, all the assembly errors can be approximately viewed as zero, but the mounting error of each precise cubic prism, less than 5″ the most of time, cannot be compensated. Consequently, the distribution of residual error after correction is still needed to be analyzed, which is in Fig. 6. In the figure, it can be seen that all of the simulation data is distributed with the same tendency as the simulation result before correction, within the red circle range of ± 40″ which is much smaller than the data before correction.

5. Correction of pointing error

5.1. Calibration of transformation matrix

In order to compensate the pointing error, all the assembly errors mentioned above need to be calibrated, namely transformation matrix. Precise cubic prisms mounted on the mechanical components are regarded as the optical reference, whose mounting status is

Table 2
Calibration result of base and outer frame.

theodolite	item	T1	T2	T3	T4
T1	azimuth angle	0	71°57′ 9″	63°9′ 3″	–
	pitch angle	90°0′ 0″	88°47′ 41″	103°31′ 33″	–
T2	azimuth angle	341°57′ 12″	0	–	34°34′ 37″
	pitch angle	91°12′ 12″	90°0′ 0″	–	107°52′ 19″
T3	azimuth angle	333°9′ 1″	–	0	13°55′ 23″
	pitch angle	76°28′ 19″	–	90°0′ 50″	89°20′ 34″
T4	azimuth angle	–	304°34′ 31″	283°55′ 22″	0
	pitch angle	–	72°7′ 35″	90°39′ 21″	90°0′ 14″

where
Ti-Ti: the collimation measurement result of Ti.
Ti-Tj: the mutual collimation measurement result of Ti between Ti and Tj.
Tj-Ti: the mutual collimation measurement result of Tj between Ti and Tj.

Table 3
Calibration result of inner frame and guiding telescope.

theodolite	item	T1	T2	T3	T4
T1	azimuth angle	0	63°43′ 38″	39°33′ 31″	–
	pitch angle	89°59′ 59"	89°25′ 47″	96°55′ 58″	–
T2	azimuth angle	333°43′ 39″	0	–	349°59′ 28″
	pitch angle	90°34′ 2″	89°59′ 58″	–	94°9′ 11″
T3	azimuth angle	302°33′ 48″	–	0	335°50′ 35″
	pitch angle	83°3′ 53″	–	90°1′ 15″	89°24′ 52″
T4	azimuth angle	–	72°59′ 48″	65°50′ 33″	0
	pitch angle	–	85°50′ 40″	90°35′ 2″	90°35′ 26″

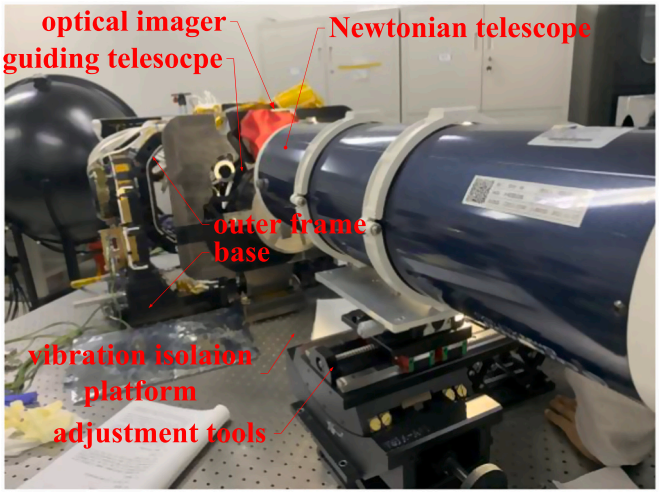

Fig. 9. Test environment.

shown in Fig. 7.

Theodolites and their working positions are shown below in Fig. 8.

5.2. Calibration results

According to the calibration method in Section 3.2, three theodolites, two TM6100s and one TM5100, are employed in the test. The calibration result of base and outer frame is presented in Table 2.

The transformation matrix from base to outer frame can be acquired according to Eq. (21), which is

$$\mathbf{T}_{\mathrm{O}}^{\mathrm{B}} = \begin{bmatrix} 0.9999999976 & 0.0000145444104 & 0.0000678739153 \\ -0.00001456020499 & 0.9999999727 & 0.0002327102347 \\ -0.00006787052882 & -0.00006787052882 & 0.9999999705 \end{bmatrix} \tag{26}$$

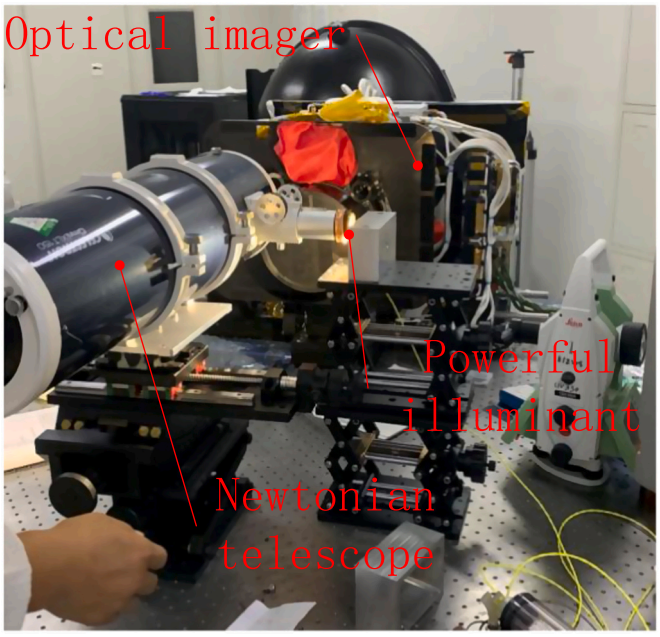

Fig. 10. Aligning and measuring process.

Table 4
Pointing error results before and after correction.

Position	Displayed error (″)	Positioning error of encoder (″)	Error before correction (″)	Error after correction (″)	Percent of compensated error	Axis
#1	- 2	- 24	- 26	0	100%	Pitch axis
#2	- 54	36	- 18	12	33.3%	
#3	- 63	31	- 32	- 8	75%	
#4	- 32	48	16	- 10	37.5%	Azimuth axis
#5	39	- 12	27	10	63%	
#6	1	23	24	-6	75%	

The angular deviation of base from outer frame can be calculated according to Eq. (23), namely

$$(\alpha_2, \beta_2, \gamma_2) = (-48.00, 13.99, -3.00) \tag{27}$$

As to inner frame and guiding telescope, the calibration result is shown in Table 3.

Similarly, the transformation matrix of inner frame and guiding telescope can be calculated as in Eq. (28) and the angular deviation is in Eq. (29).

$$\mathbf{T}_{\mathrm{G}}^{\mathrm{I}} = \begin{bmatrix} 0.999946991 & 0.00008611297594 & 0.01029601248 \\ -0.00008230878358 & 0.9999999282 & -0.0003699055482 \\ -0.01029604359 & 0.0003690384876 & 0.9999469262 \end{bmatrix} \tag{28}$$

$$(\alpha_3, \beta_3, \gamma_3) = (76.12, 2123.75, -17.76) \tag{29}$$

5.3. Correction test of pointing error

When the optical imager is working in the space, the guiding telescope needs to firstly search the target, namely the sun, on a large scale until the target lies in the center of field of view of guiding telescope. To simulate this searching process, before the guiding telescope lies a Newtonian telescope with a powerful illuminant placed on the eyepiece which is used to simulate the light rays coming from the sun. The test environment is shown in Fig. 9. The aligning and measuring process is in Fig. 10.

When the Newtonian telescope is placed before the guiding telescope with an arbitrary little angular deviation relative to the base of the imager, the guiding telescope can theoretically point to the Newtonian telescope accurately after the azimuth angle and pitch angle deviation acquired by theodolites are input into the control software. However, due to some inevitable errors brought in by manufacturing and assembly, the pointing error of the guiding telescope does exist and needs to be corrected which has been analyzed and calculated in the discussions above.

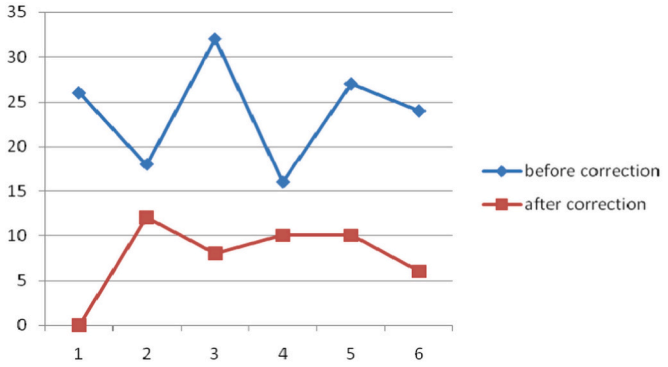

Fig. 11. Line chart of pointing error results before and after correction.

5.4. Results and discussions

In the correction test, the Newtonian telescope is placed with multiple angular deviations from the imager and test results before and after correction is recorded. The detailed test data is shown in Table 4 and the line chart in Fig. 11.

Following is the discussion about the test result. First of all, the displayed error is not the real pointing error due to the existence of positioning error of encoder. The real pointing error before correction can be gained when positioning error of encoder is taken into consideration; Secondly, as is seen in Table 4, there still exists a residual pointing error about 10″ after correction, which is caused by the systematic calibration error about 2″ of theodolite and the angular deviation of each precise cubic prism from the mechanical axis it stands for; Thirdly, when the assembly error between the optical imager and satellite platform, no more than 5″ for the most of time, is considered, the maximum of pointing error is no more than 20″, which meets the system performance requirement.

6. Conclusion

In this paper, as to an optical imager, the relation of pointing error and assembly errors of all the components is introduced and the corresponding mathematical model is established, which is of extreme helpfulness for the subsequent simulation and calibration test of pointing error. Then, the mathematical model of transformation matrix calibration between coordinate systems is set up, together with the formula of angular deviation calculation. Transformation matrices and angular deviations between base and outer frame, inner frame and guiding telescope are calibrated with help of the calibration model. Furthermore, simulation model of pointing error of the optical imager is built based on Monte-Carlo method on condition that each of all the assembly errors satisfy the normal assumption. Simulation results before and after correction are acquired demonstrating that the distribution of pointing error is within the range of $\pm 0.5^{\circ}$ before correction while $\pm 40''$ after correction, which indicates that the correction of assembly errors has a critical influence on the improvement of pointing accuracy. Last but not least, a correction test of pointing error is conducted and compensation algorithm is employed in the control system. Test results demonstrate that the maximum of compensated value is 26″ and the minimum is 6″ and the pointing accuracy has increased by 64% in average. After correction, the total pointing error of imager is no more than 20″ which meets the system performance requirement.

Declaration of Competing Interest

The authors declare that they have no known competing financial interests or personal relationships that could have appeared to influence the work reported in this paper.

References

[1] F.Q. Zhou, G.J. Zhang, J. Jiang, Three-dimensional coordinate measuring system with bino-theodolites on site, Chin. J. Mech. Eng. 40 (1) (2004) 165–169.
[2] J. Fu, W. Chu, R. Dixon, et al., Three-dimensional image correction of tilted samples through coordinate transformation, Scanning 30 (1) (2008) 41–46.
[3] R. Zhang, Y.Y. Zhang, Z.J. Liang, J.B. Jiang, T. Ling, High-precision calibration method for shear ratio based on the shearing wavefront feature extraction of a phase plate, Appl. Opt. 57 (2018) 5121–5129.
[4] K.V. Chellappan, E. Erden, H. Urey, Laser-based displays: a review, Appl. Opt. 49 (2010) F79–F98.
[5] B. Wu, X.Y. Su, A novel precise guiding method for visual guiding theodolite measurement in volume space, Optik 126 (2015) 3969–3973.
[6] X.H. Zhang, Z.K. Zhu, Y. Yuan, et al., A universal and flexible theodolite-camera system for making accurate measurement over large volumes, Opt. Lasers Eng. 50 (2012) 1611–1620.
[7] A.B. Forbes, B. Hughes, W.J. Sun, Comparison of measurements in co-ordinate metrology, Measurement 42 (2009) 1473–1477.
[8] J. Schlarp, E. Csencsics, G. Schiter, Optical scanning of laser line sensors for 3D imaging, Appl. Opt. 57 (2018) 5242–5248.
[9] J.H. Kang, B. Wu, X.D. Duan, T. Xue, A novel calibration method of articulated laser sensor for trans-scale 3D measurement, Sensors 19 (2019) 1083.
[10] L.Q. Ma, L.D. Wang, T.Z. Cao, et al., A large-scale laser plane calibration system, Meas. Sci. Technol. 18 (2007) 1768–1772.
[11] X.B. Liang, J. Zhou, W.L. Ma, Method of distortion and pointing correction of a ground-based telescope, Appl. Opt. 58 (2019) 5136–5142.
[12] C. Xu, W. Han, D.Z. Wang, D.Q. Huang, P.F. Yuan, Modeling and correction for the optical axis pointing error of an airborne electro-optical platform, Appl. Opt. 58 (2019) 6455–6463.

[13] C.L. Liu, J.H. Liu, Y.M. Song, H.D. Liang, A novel system for correction of relative angular displacement between airborne platform and UAV in target localization, Sensors 17 (2017) 510.
[14] S.H. Ding, X.G. San, S.J. Gao, Y.X. Ni, J. Wang, Laser communication pointing errors caused by bending deformation of the altitude axis of a T-shaped altitude-azimuth mount, Appl. Opt. 58 (30) (2019) 8141–8147.
[15] L.Y. Tan, Y.W. Song, J. Ma, S.Y. Yu, Q.Q. Han, Y.J. Jiang, J. Wang, S. Fu, Pointing error due to temperature distribution of SiC reflectors in inter-satellite laser communication, Appl. Opt. 49 (2010) 4168–4174.
[16] J. Ma, G.Y. Lu, S.Y. Yu, L.Y. Tan, Y.L. Fu, F.J. Li, Fiber coupling efficiency for satellite and space to ground downlinks with pointing errors, Optik 202 (2020) 1–15.
[17] W.G. Alheadary, K.H. Park, M.S. Alouini, Performance analysis of multihop heterodyne free-space optical communication over general Malaga turbulence channels with pointing error, Optik 151 (2017) 34–47.
[18] K.O. Odeyemi, P.A. Owolawi, V.M. Srivastava, Optical spatial modulation over Gamma-Gamma turbulence and pointing error induced fading channels, Optik 147 (2017) 214–223.
[19] K. Prabu, D.S. Kumar, R. Malekian, BER analysis of BPSK-SIM-based SISO and MIMO FSO systems in strong turbulence with pointing errors, Optik 125 (2014) 6413–6417.
[20] A. Sharma, J. Malhotra, S. Chaudhary, V. Thappa, Analysis of 2×10Gbps MDM enabled inter satellite optical wireless communication under the impact of pointing errors, Optik 227 (2021) 1–7.
[21] L.J. Johnson, R.J. Green, M.S. Leeson, Underwater optical wireless communication depth-dependent beam refraction, Appl. Opt. 53 (2014) 7273–7277.
[22] X.Y. Xue, Y.G. Gao, G.Y. Han, S. Shao, J. Qiao, Total correction method of pointing error for level mounting theodolites, Opt. Precis. Eng. 19 (2011) 1524–1530.
[23] Y. Zhou, Y. Lu, M. Hei, G. Liu, D. Fan, Pointing error analysis of Risley-prism-based beam steering system, J. Appl. Opt. 53 (2014) 5775–5783.
[24] L.J. Yan, Y.M. Huang, Y.H. Zhang, Using Allan variance-based semi-parameter model to calibrate pointing errors of alt-az telescopes, Appl. Sci. 8 (2018) 614.
[25] Q.J. Tang, X.J. Wang, Q.P. Yang, Static pointing error analysis of electro-optical detection systems, Proc. Inst. Mech. Eng. B 230 (2016) 593–600.